4-Phenylbutyric Acid Activates an NF-κB - Egr-1 Axis to Control Myoblast Proliferation and ECM Gene Expression Profiles

Kana Tominaga[1*], Naoomi Tominaga[2]

1. Division of Neuropsychiatry, Department of Neuroscience, Yamaguchi University Graduate School of Medicine, 1-1-1 Minami-kogushi, Ube, Yamaguchi, 755-8505, Japan

2. Department of Laboratory Medicine, Faculty of Health Sciences, Yamaguchi University Graduate School of Medicine, 1-1-1 Minamikogushi, Ube, Yamaguchi, 755-8505, Japan

Corresponding author:

Kana Tominaga, Ph.D.

Division of Neuropsychiatry, Department of Neuroscience,

Yamaguchi University School of Medicine

1-1-1 Minami-kogushi, Ube, Yamaguchi, 755-8505, Japan

Email: kanat@yamaguchi-u.ac.jp

TEL: +81-836-22-2255

Abstract

Myoblast proliferation and differentiation are tightly controlled by epigenetic mechanisms, yet how clinically used epigenetic modulators influence myogenic cell fate remains incompletely understood. Here, we demonstrate that the histone deacetylase inhibitor and chemical chaperone 4-phenylbutyric acid (4-PBA) selectively promotes myoblast proliferation without inducing differentiation in C2C12 cells. Mechanistically, 4-PBA increases histone H3 acetylation at lysines 18 and 27 via downregulation of HDAC5, resulting in activation of NF-κB p65. Chromatin immunoprecipitation identifies early growth response 1 (Egr-1) as a direct transcriptional target of NF-κB p65. Transcriptomic analyses reveal that Egr-1 regulates extracellular matrix- and myogenesis-associated gene programs, including multiple collagen genes. Consistently, 4-PBA induces a transcriptional signature that significantly overlaps with Egr-1-dependent gene expression. Functional studies further establish that the NF-κB p65 - Egr-1 axis is required for 4-PBA-mediated transcriptional remodeling in proliferating myoblasts. Together, these findings uncover an epigenetic mechanism by which 4-PBA modulates myoblast proliferation through HDAC5-dependent histone acetylation and NF-κB p65 - Egr-1 driven transcriptional programs, providing insight into how epigenetic therapeutics influence skeletal muscle cell behavior.

Highlight

- 4-PBA enhances murine myoblast proliferation independently of differentiation induction.
- 4-PBA enhances H3K18 and H3K27 acetylation through downregulation of HDAC5.
- NF-κB p65 activates Egr-1 by directly binding to the Egr-1 promoter region.
- 4-PBA stimulates the HDAC5 - NF-κB p65 - Egr-1 axis drives extracellular matrix-related gene profiles.

Main Text

Introduction

Myoblasts are proliferative precursor cells derived from muscle satellite cells[1,2] Satellite cells are skeletal muscle stem cells that reside in a quiescent state beneath the basal lamina of muscle fibers[3,4]. In response to muscle injury or growth signals, satellite cells become activated and give rise to myoblasts, which proliferate and subsequently differentiate to form new muscle fibers (myotubes/myofibers)[5,6]. This process is essential for skeletal muscle growth, regeneration, and repair and represents a promising therapeutic target for muscle-related diseases[7,8].

Histone acetylation plays a central role in the proliferation and the differentiation of myoblasts[9]. During differentiation, histone acetyltransferases (HATs) are recruited to the promoters and enhancers of muscle-specific genes, leading to increased acetylation of histone marks such as H3K9ac and H3K27ac[10–12]. This epigenetic remodeling activates key myogenic genes, including Myog, myosin heavy chain (Myh), and muscle creatine kinase[10,13]. The myogenic transcription factor MyoD recruits HATs such as p300/CBP and PCAF to muscle gene loci, enhancing chromatin accessibility and reinforcing muscle-specific transcription[14,15]. Concurrently, histone deacetylases (HDAC) are displaced from muscle gene promoters but remain associated with cell cycle-related genes to ensure permanent withdrawal from proliferation[16,17]. Pharmacological inhibition of HDAC increases histone acetylation and can accelerate myoblast differentiation, underscoring the importance of balanced acetylation in myogenesis[18].

4-PBA is currently used clinically to treat patients with urea cycle disorders under the names Buphenyl (sodium phenylbutyrate) and Ravicti (glycerol phenylbutyrate)[19]. Its primary mechanism of action involves binding toxic ammonia to provide an alternative pathway for its elimination[19,20]. In addition, 4-PBA functions as a chemical chaperone that reduces endoplasmic reticulum (ER) stress and prevents protein aggregation[21–23]. 4-PBA has attracted interest for disorders involving protein misfolding, such as cystic fibrosis with the ΔF508 *CFTR* mutation and vascular ehlers danlos syndrome with *COL3A1* mutations[24–26]. Previous studies have shown that 4-PBA treatment restores the membrane localization of pathogenic mutant

65 dysferlin (Dysf) in cultured myotubes and myofibers obtained from dysferlinopathy model mice, suggesting
66 that 4-PBA rescues dysferlin from aggregation or degradation in the endoplasmic reticulum (ER)[27]. 4-PBA
67 is also recognized as a HDAC inhibitor, adding an epigenetic mechanism to its therapeutic effects. During
68 cardiomyogenesis, 4-PBA promotes early cardiac differentiation via increased histone acetylation but
69 inhibits late-stage differentiation by maintaining the expression of pluripotency genes such as *Oct4, Nanog,*
70 and *Sox2*, demonstrating that HDAC regulation exerts context-dependent effects[28]. In the case of cancer, 4-
71 PBA inhibits tumor cell proliferation by increasing histone acetylation, inducing epithelial-mesenchymal
72 transition, and promoting acetyl-H3-mediated transcription[29–31]. Hence, these effects suggest that 4-PBA
73 may alleviate ER stress caused by misfolded proteins and enhance protein homeostasis. In contrast, despite
74 the clinical response to 4-PBA in diseases caused by misfolded proteins, little is known about its role as an
75 HDAC inhibitor of myogenesis.

76 Our study demonstrated that 4-PBA regulates myoblast differentiation through epigenetic and
77 transcriptional mechanisms. In C2C12 myoblasts, chromatin immunoprecipitation assays revealed that NF-
78 κB p65 directly binds to the Egr-1 promoter, identifying Egr-1 as a transcriptional target of the NF-κB
79 signaling pathway. During myogenesis, 4-PBA treatment markedly increased histone H3 acetylation,
80 especially at Lys18 and Lys27, and downregulated HDAC5 expression, resulting in increased Egr-1 and
81 p65 expression. Moreover, transcriptome analysis revealed that Egr-1 regulated extracellular matrix
82 (ECM)-related genes, including multiple collagen genes. This study revealed that 4-PBA acts as an HDAC
83 inhibitor that contributes to myogenic homeostasis by regulating the NF-κB - Egr-1 axis.

84

85 **Results**

86 **4-PBA induces cell proliferation in murine myoblasts.**

87 To confirm the effects of 4-PBA on myoblast differentiation, we first examined morphological changes in
88 C2C12 myoblasts following 4-PBA treatment. C2C12 myoblasts were cultured under differentiation

89 conditions and treated with 4-PBA for four days (Figure S1A). Myotube formation was then assessed by
90 measuring the myofusion index and the protein levels of myosin heavy chain 1 (Myh1), a major contractile
91 protein, using immunofluorescence analysis (Figure 1A). We observed a significant decrease in the fusion
92 index and reduced Myh1 expression in 4-PBA-treated cells compared with control cells (Figure 1B). We
93 next examined the protein expression of myogenin (Myog), a myogenic transcription factor, and Dysf, a
94 marker of mature muscle fibers, under 4-PBA-treated conditions (Figure 1C). The results showed that 4-
95 PBA significantly suppressed the induction of Myog at all stages (day 1 - 4) and Dysf at later stages (day 3
96 - 4) of myotube differentiation (Figure 1D). On the other hand, RNA-seq analysis of myoblast
97 differentiation from day 0 to day 4 indicated that there was no difference in the expression of myoblast
98 differentiation-related genes between DMSO- and 4-PBA-treated cells (Figure S1B - S1D). These results
99 suggest that 4-PBA suppresses myogenic differentiation primarily through post-transcriptional,
100 translational, or protein stability-related mechanisms rather than by regulating myogenic gene expression
101 at the mRNA level.

102 To identify the biological pathways affected by 4-PBA treatment in myoblasts, we analyzed RNA-seq data
103 (GSE315556) from C2C12 myoblasts treated with 4-PBA under differentiation conditions for four days.
104 KEGG pathway analysis revealed that genes upregulated by 4-PBA treatment were primarily associated
105 with cell proliferation-related pathways (Figure 1E and Data S1). Three representative pathways were
106 visualized to facilitate interpretation (Figure 1F). To validate the RNA-seq results indicating enhanced
107 proliferation, we examined cell proliferation in C2C12 myoblasts treated with 4-PBA or DMSO as a control.
108 Compared with DMSO-treated cells, C2C12 myoblasts treated with 4-PBA showed significantly increased
109 proliferation after four days (Figure 1G), suggesting that compared with myoblast differentiation, 4-PBA
110 promotes cell proliferation.

111 **4-PBA induces Egr-1 expression during myogenesis.**

112 4-PBA acts as an HDAC inhibitor, thereby increasing histone acetylation and consesquently promoting
113 gene expression. Therefore, to identify genes upregulated by 4-PBA treatment during myogenic

114 differentiation, we compared the gene expression profiles of 4-PBA-treated C2C12 myoblasts with those
115 of DMSO-treated or undifferentiated (baseline) cells via RNA-Seq (GSE315556, Data S2). Principal
116 component analysis (PCA) revealed that compared with the baseline treatment, the 4-PBA and DMSO
117 treatments caused significant changes in the state, after which the 4-PBA-treated C2C12 myotubes formed
118 a distinct cluster that was clearly separated from the DMSO treatment (Figure 2A). These results indicated
119 a strong and consistent global transcriptional change caused by 4-PBA treatment during myogenesis.
120 Transcriptomic analysis revealed that only two genes, Egr-1 and Fos, were differentially expressed genes
121 (DEGs) based on the criteria of | log2-fold change | > 1.2 and $p < 0.01$ (Figure 2B and 2C). The mRNA
122 expression levels of both genes were greater in 4-PBA-treated C2C12 myotubes than in DMSO-
123 treated cells or baseline controls (Figure 2D). At the protein level, Egr-1 expression markedly increased in
124 4-PBA-treated C2C12 cells compared with that in DMSO-treated and control cells, particularly during
125 the early stages of differentiation (Figure 2E and 2F). In contrast, Fos protein expression did not
126 significantly differ between 4-PBA- and DMSO-treated C2C12 cells. These findings indicated that Egr-1
127 is a primary and functionally relevant target of 4-PBA in the transformation of C2C12 myoblasts to
128 myotubes.

129 **4-PBA modulates the NF-κB p65-dependent expression of murine myoblasts.**

130 To identify the signaling pathway that regulates Egr-1 expression, we focused on the Erk pathway and the
131 NF-κB p65 signaling pathway. Some studies have shown that 4-PBA inhibits the activation of both
132 pathways in cells, primarily through its ability to reduce ER stress. We treated C2C12 myoblasts with 1
133 mM 4-PBA or DMSO for four days during myotube differentiation and then evaluated the phosphorylation
134 of Erk or NF-κB p65. Erk1/2 phosphorylation remained unchanged following 4-PBA or DMSO treatment,
135 whereas NF-κB p65 expression and phosphorylation increased in 4-PBA-treated C2C12 cells from the early
136 stages of differentiation (Figure 3A and 3B). To confirm whether Egr-1 expression is regulated by the
137 canonical NF-κB signaling pathway, we analyzed the protein levels of Egr-1 in 4-PBA-treated C2C12
138 myoblasts treated with dehydroxymethylepoxyquinomicin (DHMEQ), an NF-κB p65 inhibitor, for 24

139 hours. Immunoblotting revealed that Egr-1 protein levels increased in response to 4-PBA treatment but
140 decreased in response to the addition of DHMEQ (Figure 3C and 3D). NF-κB p65 may act as a transcription
141 factor that regulates Egr-1.

142 Putative NF-κB (p65) binding sites were identified based on the established κB consensus sequence (5′-
143 GGGRNNYYCC-3′) in the *Homo sapiens* (GRCh38). However, within the EGR promoter region, a
144 consensus NF-κB (p65) binding motif was identified in the human sequence, whereas no corresponding
145 motif was detected in the mouse sequence. To identify NF-κB p65 binding sites that control Egr-1
146 transcription in the *Mus musculus* genome (GRCm39), we predicted putative NF-κB p65 binding sites
147 within the −2000 bp promoter region of *Egr-1* using the JASPAR database (Figure 3E and S2A). We
148 designed two primer pairs encompassing the predicted motifs (P1) and two primer pairs flanking regions
149 adjacent to the motifs (P2 and P3) to assess DNA enrichment (Figure 3F and S2B). ChIP–qPCR analysis
150 revealed that the P1 fragment was directly bound by NF-κB p65, whereas the other fragments (P2 and P3)
151 were not enriched (Figure 3G). These results demonstrate that NF-κB p65 directly binds to the *Egr-1*
152 promoter, specifically at the P1 region (CTGGAATCCC), indicating that *Egr-1* is a direct transcriptional
153 target of NF-κB p65. Moreover, compared with DMSO-treated C2C12 myoblasts, 4-PBA-treated C2C12
154 myoblasts exhibited significantly increased binding of NF-κB p65 to the *Egr-1* promoter, suggesting that
155 this treatment enhances NF-κB-mediated transcriptional regulation of Egr-1, potentially contributing to
156 altered *Egr-1* gene expression under these conditions.

157 **4-PBA induced the acetylation of histone H3 but not NF-κB p65.**

158 To determine whether 4-PBA treatment directly affects histone acetylation, we examined the acetylation
159 status of histone H3 at residues H3K9, H3K14, H3K18, H3K27, and H3K56 during myogenesis by
160 immunoblotting. Histone H3 acetylation markedly increased at the early stage of differentiation following
161 inhibitor treatment, particularly at H3K18 and H3K27 (Figure 4A and 4B). These results suggest that
162 HDAC inhibition by 4-PBA alters the acetylation status of specific histone lysine residues.

163 Other groups have reported that 4-PBA directly interacts with NF-κB p65 and regulates its acetylation[32].
164 We therefore evaluated the acetylation of NF-κB p65 at Lys310 during C2C12 myoblast differentiation by
165 immunoblotting. The acetylation of NF-κB p65 at Lys310 increased during myoblast differentiation;
166 however, inhibitor treatment reduced p65 acetylation (Figure 4C and 4D). Consistently,
167 coimmunoprecipitation using an antibody against p65 in C2C12 myotubes revealed that inhibitor treatment
168 decreased NF-κB p65 acetylation (Figure 4E). These findings indicate that despite its strong effects on
169 histone acetylation, 4-PBA does not increase and instead reduces NF-κB p65 acetylation in C2C12 cells.

170 **4-PBA-induced Hdac5 expression negatively regulates Egr-1 expression during myogenesis.**

171 4-PBA suppresses Hdac5 protein expression, leading to the hyperacetylation of histone H3 in C2C12
172 myotubes[33]. However, it is still unclear which class of HDACs is the primary target of 4-PBA. To
173 investigate which classes of HDACs are predominantly downregulated by 4-PBA treatment during
174 myogenesis, we first evaluated the gene expression of all the HDACs in C2C12 myotubes treated with 1
175 mM 4-PBA compared with those treated with DMSO. We observed significantly lower Hdac5 gene
176 expression in C2C12 myotubes than in DMSO control myotubes (Figure 5A and Data S3). Hdac5
177 expression increases during the early stages of differentiation, confirming that Hdac5 expression is affected
178 by the formation of immature myotubes (Figure 5B and 5C). In contrast, 4-PBA treatment reduced Hdac5
179 expression during myogenesis, which is consistent with the RNA-seq data. Together, these results suggest
180 that Hdac5 is a key epigenetic regulator during early myogenesis and that 4-PBA treatment suppresses its
181 expression, potentially leading to altered histone acetylation and dysregulated transcriptional programs
182 during muscle differentiation.

183 We next confirmed that Hdac5 is directly related to Egr-1 expression. Depletion of *Hdac5* mRNA
184 expression significantly increased the *Egr-1* mRNA level in 4-PBA-treated C2C12 cells (Figure 5D),
185 suggesting that Hdac5 negatively regulates *Egr-1* expression. We next performed immunoblotting analysis
186 to examine the protein levels of Egr-1 and NF-κB p65, as well as histone H3 acetylation at Lys18 and Lys27,
187 which are known to be upregulated by 4-PBA treatment. The results revealed that the protein expression of

188 Egr-1 and NF-κB p65, along with the acetylation of histone H3 at Lys18 and Lys27 (Figure 5E and 5F),
189 was significantly greater in *Hdac5*-knockdown cells than in control cells. These results suggest that HDAC5
190 knockdown in C2C12 cells enhances histone H3 acetylation and activates NF-κB signaling and Egr-1
191 expression, indicating that the mechanism is similar to that of 4-PBA.

192 **4-PBA regulated ECM organization-related genes via Egr-1.**

193 To investigate the mechanism through which Egr-1 affects myogenic differentiation, the gene expression
194 profiles of C2C12 cells with or without 4-PBA were determined via RNA-Seq. GO enrichment analysis
195 revealed that the significantly enriched functional categories among the upregulated genes included positive
196 regulation of external encapsulating structure organization, extracellular matrix organization, extracellular
197 structure organization and collagen aggregation (Figure 6A and Data S4). Furthermore, network analysis
198 using GO enrichment revealed genes significantly involved in extracellular matrix (ECM) structural
199 constituent, integrin binding and cell adhesion molecule binding (Figure 6B). In particular, the expression
200 of collagen-related genes, which encode structural components of the extracellular matrix, increased during
201 myoblast differentiation (Fig. S3A and Data S5), suggesting that ECM-associated genes play important
202 roles in muscle differentiation.

203 We next identified the ECM-related genes regulated by Egr-1 expression that were upregulated by 4-PBA
204 treatment in C2C12 cells. A Venn diagram was constructed to examine the intersection between Egr-1
205 target genes based on the ENCODE Transcription Factor Targets Dataset[34] and ECM structural components
206 (GO: 0005201), indicating that a total of 36 common genes were identified (Figure 6C). On the other hand,
207 we found that there were no genes common between Egr-1 target genes and categories for the adhesion
208 molecule binding (GO:0050839), integrin binding (GO:0005178), and heparin binding (GO:0008201) that
209 the network analysis using GO enrichment reveled (Figure S3B). To identify the genes linking 4-PBA to
210 the upregulation of ECM via Egr-1 expression, we displayed the main representative up-regulated genes on
211 a heatmap, and the expression of Egr-1 target genes by 4-PBA increased gradually from left to right (Figure
212 6D and Data S6). Changes in gene expression following Egr-1 knockdown were confirmed using qRT-PCR.

213 Several extracellular matrix (ECM)-related genes, including collagen type XI alpha 1 (Col11a1), collagen
214 type XXVII alpha 1 (Col27a1), collagen type IV alpha 1 (Col4a1), and collagen type IV alpha 2 (Col4a2),
215 as well as genes involved in the production of collagen, such as cartilage oligomeric matrix protein (Comp),
216 and myogenesis-related genes, including matrilin-2 (Matn2) and nidogen-2 (Nid2), a crucial BM protein in
217 muscle, were among the most significantly downregulated in Egr-1-transfected C2C12 myoblasts compared
218 with those in siControl-transfected cells or at baseline levels (Figure 6E). Moreover, the expression of these
219 genes was significantly greater in C2C12 myoblasts treated with the inhibitor than in those treated with
220 DMSO (Figure 6F). Similar downregulation of these genes was also observed in siHdac5-treated cells
221 (Figure S3C). Overall, these results suggest that 4-PBA promotes ECM remodeling and the expression of
222 muscle-related genes and that Egr-1 is involved in regulating the expression of these genes.

223

224 **Discussion**

225 Although significant progress has been made in understanding muscle differentiation, many of the
226 underlying mechanisms remain unresolved. Here, we report that 4-PBA regulates myoblast differentiation,
227 cell proliferation, and ECM remodeling via epigenetic and transcriptional mechanisms, advancing our
228 understanding of muscle pathology and facilitating the development of novel therapeutic strategies for
229 muscle-related diseases such as sarcopenia and muscular dystrophy.

230 We found that 4-PBA acts as an epigenetic regulator during myoblast differentiation. Transcriptomic
231 screening and immunoblotting analysis revealed that histone H3 acetylation (H3K18ac and H3K27ac)
232 increased during early differentiation, supporting the role of 4-PBA as an effective inhibitor of Hdac5 in
233 C2C12 myoblasts. We demonstrate that compared with many HDAC inhibitors that reinforce muscle-
234 specific transcription, 4-PBA inhibits myoblast differentiation and the expression of the myogenic-related
235 genes *Myod* and *Dysf* to promote muscle differentiation. Importantly, 4-PBA selectively induced the
236 expression of NF-κB p65 via inhibition of Hdac5 expression. NF-κB plays complex roles in skeletal muscle
237 differentiation through opposing signaling pathways[35]. The canonical NF-κB signaling pathway, via

238 RelA/p65, IKKβ, and IKKγ, and is a key transcription factor that generally promotes muscle cell
239 proliferation, especially in skeletal muscle stem cells (MuSCs) after chronic injury[36–38]. We propose that 4-
240 PBA promotes cell proliferation by activating the NF-κB signaling pathway, thereby contributing to
241 myoblast expansion during early myogenesis following injury.

242 We identified HDAC5 as a key epigenetic regulator during early myogenesis and suggest that its
243 suppression by 4-PBA contributes to altered histone acetylation and transcriptional dysregulation. We also
244 suggest that 4-PBA is a target for the acetylation of histone H3 but not NF-κB p65 directly through HDAC5
245 inhibition. In fact, fasting or several types of muscular dystrophy increase p65 acetylation at Lys-310,
246 activating NF-κB and contributing to muscle atrophy[39]. Acetylated NF-κB p65 also promotes the expression
247 of inflammatory genes, a hallmark of muscle wasting[39,40]. In acute muscle injury, inflammation is necessary
248 but must be precisely resolved to avoid chronic damage[41]. Notably, long-term 4-PBA treatment during
249 myogenesis reduces the phosphorylation of NF-κB p65 gradually as myotubes mature, which is activated
250 in the early stage (Figure 3A and B). These findings suggest that myogenesis-related factors may contribute
251 to a negative feedback loop that controls the accumulation of NF-κB p65 signaling. This process contributes
252 to the suppression of excessive activation of the NF-κB signaling pathway. 4-PBA can act downstream of
253 many signaling cascades, allowing regeneration to proceed without broadly activating NF-κB-driven
254 inflammatory pathways that can exacerbate tissue damage.

255 We identified Egr-1 expression as a key factor that alternates between cell proliferation and differentiation
256 in myoblasts, and we functionally characterized the regulation of Egr-1 expression by NF-κB p65. We
257 found that 4-PBA induces Egr-1-regulated extracellular matrix (ECM)- and collagen-related gene
258 expression. Collagen provides structural stability to muscle fibers and the surrounding connective tissues,
259 thereby contributing to myoblast differentiation, fusion, and proper structural organization[42]. In most
260 muscular dystrophies, the accumulation of collagen, particularly type I, type III and type IV collagens, is
261 markedly increased[43–46]. Excessive collagen deposition within the ECM, which is produced mainly by
262 fibroblasts, progressively leads to fibrosis and impaired muscle function. In contrast, specific collagen

263 types—primarily nonfibrillar collagens—serve as essential components of the MuSC microenvironment
264 and regulate their behavior. In our study, we detected increased expression of Col27a1, Col4a1, and Col4a2,
265 which are known ECM components that support normal muscle development, regeneration, and resistance
266 to mechanical stress. Notably, Col27a1 is expressed in the MuSC niche, suggesting a potential role in
267 regulating the local microenvironment[2]. Type IV collagen is a key component of the basement membrane
268 (BM), which surrounds satellite cells together with laminin and interacts with surface α7/β1 integrins[47,48].
269 4-PBA induces the expression of genes involved in collagen production, namely, Matn2 and Nid2. Matn2
270 functions as a key regulator of myogenic program initiation by modulating BMP7 and integrin α5 signaling,
271 inducing the expression of the Cdk inhibitor p21, and activating myogenic genes, including Nfix, MyoD,
272 and Myog[52]. Nid2 has been detected in conditioned media from differentiating human myoblasts by mass
273 spectrometry, which suggests that it is secreted as a soluble protein during myogenesis[49,50]. Nid2 is also a
274 component of the muscle basal lamina and plays an important role in neuromuscular junction
275 development[51,52]. Collectively, these results indicate that 4-PBA promotes ECM gene expression via the
276 NF-κB p65 - Egr-1 signaling axis, thereby facilitating the expansion of undifferentiated muscle cells and
277 generating replacement cells capable of responding to injury-associated cues. Moreover, in 4-PBA-treated
278 skeletal muscle cells, these specialized ECMs may regulate signaling activities and maintain satellite cells
279 in an undifferentiated state.

280 HDAC inhibitors such as trichostatin A (TSA), sodium butyrate (NaB), and valproic acid (VPA) have been
281 shown to influence myoblast differentiation by increasing histone acetylation and activating muscle-
282 specific gene expression in muscular atrophy and muscular dystrophy models[53–55]. Recently, givinostat,
283 known as DUVYZAT, which is an HDAC inhibitor for HDAC1 and HDAC3, was approved for patients
284 with Duchenne muscular dystrophy and has the potential to restore dystrophin expression, reduce
285 inflammation, and preserve muscle integrity[18]. Previous studies have shown that 4-PBA helps to restore the
286 membrane localization of the DYSF protein and repair the sarcolemma in a mouse model of
287 dysferlinopathy[27]. Our data also indicate that 4-PBA controls cell proliferation and differentiation by

288 targeting histone H3 without hyperactivation of inflammatory pathways, including the NF-κB signaling
289 pathway. Collectively, these findings, together with our present results, suggest that 4-PBA plays an
290 important role in myogenic differentiation after injury through the regulation of gene expression related to
291 ECM remodeling and the alleviation of ER stress, potentially contributing to the prevention of muscle
292 diseases. In summary, this work establishes a role for the HDAC inhibitor 4-PBA in maintaining muscle
293 homeostasis and identifies Egr-1 expression and NF-κB p65 as key molecules for promoting myoblast
294 proliferation. Future studies are warranted to determine such potential clinical applications.

295

296 **Limitation of the study**

297 Despite the mechanistic insights gained in this study, several limitations should be acknowledged, along
298 with potential strategies to address them in future work.

299 First, Although we identified HDAC5 inhibition as a primary mechanism underlying 4-PBA-mediated
300 effects on histone acetylation, NF-κB signaling, and ECM gene expression, 4-PBA is a multifunctional
301 compound with pleiotropic biological activities. Our findings indicate that chemical chaperone activity and
302 ER stress alleviation may act in parallel with epigenetic regulation. Dissecting these mechanisms will
303 require complementary genetic approaches, including ER stress-specific modulators.

304 Second, our analysis of NF-κB signaling focused primarily on early myogenesis, where transient activation
305 appears to promote myoblast proliferation. However, prolonged or excessive NF-κB activation is associated
306 with chronic inflammation and muscle wasting. Long-term in vivo studies are therefore needed to determine
307 whether 4-PBA maintains a beneficial balance between regenerative signaling and inflammatory resolution
308 during aging or chronic muscle disease.

309 Finally, although we observed increased expression of ECM- and collagen-related genes associated with a
310 supportive satellite cell niche, we did not directly assess ECM architecture, biomechanical properties, or
311 interactions with fibroblasts and immune cells. Future studies combining histological, biophysical, and

312 single-cell approaches will help clarify whether 4-PBA-induced ECM remodeling favors regeneration
313 without promoting fibrosis.

314 Together, addressing these limitations will be critical for translating 4-PBA-based strategies toward safe
315 and effective therapies for muscle injury and degenerative diseases.

316

317 **Methods**

318 *Cell culture*

319 C2C12, a myoblast cell line, were purchased from the American Type Culture Collection. Cells were
320 cultured in growth medium containing Dulbecco's Modified Eagle Medium (DMEM; Genesee Scientific)
321 containing 10 % fetal bovine serum (FBS, Avantor Seradigm), 100 units/ml penicillin, and 100 μg/ml
322 streptomycin (Tharmo Fisher Scientific). Cell lines were cultured in a humidified atmosphere at 37 °C in
323 5 % CO_2, and the culture medium was changed every 2 days. When cells reached subconfluence, they were
324 rinsed in phosphate-buffered saline (PBS, pH 7.4, Genesee Scientific), trypsinized with 0.25 % trypsin-
325 EDTA solution (Corning) for 5 min at 37°C, and passaged at ratios of 1:4 - 1:8.

326 To induce the differentiation and cell fusion, cells were washed with PBS, then changed to differentiation
327 medium containing DMEM containing 5 % horse serum, and 100 units/ml penicillin, and 100 μg/ml
328 streptomycin. The differentiation medium was changed every day.

329 *Small interfering RNA (siRNA)*

330 For knockdown of Hdac5 or Egr-1, we used Silencer Select Mouse Hdac5 (Assay ID s67423) or Mouse
331 Egr-1 (Assay ID s65378) purchased from Invitrogen. C2C12 myoblasts were seeded at a density of 1×10^5
332 cells/well into a 6-well plate and incubated with siRNAs (5 or 15nM) and Lipofectamine RNAiMAX
333 transfection reagent (Invitrogen) according to the manufacturer's protocol. The control was Silencer Select
334 Negative Control No. 1 siRNA. siRNA-transfected cells were incubated at 37°C in 5% CO_2 until the assay.
335 Representative data from three independent experiments.

336 *RNA sequence*

337 C2C12 myoblasts were plated at 7.0×10^5 cells in 60 mm dishes in growth medium (DMEM with 10% FBS
338 and penicillin/streptomycin). Once confluent, media was changed to differentiation medium (DMEM with
339 2% HS and penicillin/streptomycin) with 1mM 4-PBA or DMSO as control and left to differentiate for
340 4 days. Differentiation medium was replenished daily.

341 We purified total RNA using an Maxwell RSC simply RNA Cell Kit (Promega, AS1390), followed
342 by DNase treatment and assess the RNA purity using a Tapestation 4200 High Sensitivity RNA (Agilent
343 Technologies, 5067-5579).

344 RNA-seq analysis was performed as previously described. We used The NEBNext Poly(A) mRNA
345 Magnetic Isolation Module (New England BioLabs, E7490) and NEBNext Ultra II Directional RNA
346 Library Prep Kit for Illumina (New England BioLabs, E7760) to generate cDNA libraries for Illumina
347 sequencing. we used An Agilent 4200 TapeStation (Agilent, D1000) to evaluate the quality and
348 concentration of the libraries. Confirmed libraries were mixed in equal molar amounts for clustering and
349 sequencing on an Illumina NovaSeq 6000 DNA sequencer with a 50-bp, using NovaSeq 6000 S1 Reagent
350 Kit V1.5 (Illumina). We used CLC Genomics Workbench 23.0.2 for data analysis. Trimmed reads were
351 mapped to the *Mus musculus* (GRCm39) release-110 database and counted according to default settings
352 using a CLC Genomics Workbench (Qiagen). mRNA abundance is expressed as the log2-transformed
353 transcripts per million plus one. We use the R package seqinr to read the FASTA file.

354 *Immunoblotting*

355 Cultured cells were denatured with SDS sample buffer (Nacalai Tesque) at 99 °C for 5 min. Lysates were
356 loaded 10 μg protein/lane to run SDS-PAGE. The proteins were separated by SDS-PAGE and transferred
357 to polyvinylidene fluoride (PVDF) membranes. The membranes were blocked with Block Ace (Bio-rad)
358 and incubated at room temperature for 1 hour with primary antibodies (Table S1). After washing PBS
359 containing 0.1% Tween 20, the membranes were incubated at room temperature for 1 hour with horseradish

360 peroxidase (HRP)-conjugated anti-rabbit or anti-mouse IgG (CST) as secondary antibodies. Signals were
361 developed using an Immobilon Western Chemiluminescent HRP Substrate (Cytiva) and examined using an
362 Amasham imaging system (GE Healthcare). To analyze the intensity of bands, we used Fiji (ImageJ 1.53t).

363 *Co-immunoprecipitation (Co-IP)*

364 The cell lysates were extracted from the treated C2C12 myotubes by use of RIPA lysis buffer, and then
365 cultured overnight with specific antibodies against p65 and IgG (negative control) in constant speed at 4 °C.
366 Following mixing with magnetic-beads (Cytiva), the antigen-antibody mixture was acquired. After washing
367 thrice in IP lysis buffer, immunoblotting was conducted for the eluted proteins. See Table S1 for primer
368 antibodies details.

369 *Immunofluorescence*

370 The cultured cells were fixed in pre-child 4% parahormardehid at room tempreture for 10 min. After
371 washing in PBS containing 0.1 % Triton X-100 for 5 min, cells were incubated with 3 % bovine serum
372 albumin (BSA, Sigma) at room temperature for 60 min to block non-specific binding and then incubated
373 with Anti-Myh1 antibody (Sigma-Aldrich, ZRB1214) as a primary antibody at room temperature for 1 hour.
374 After washing with PBS, the cells and sections were incubated with an Alexa Fluor 488 Goat Anti-Rabbit
375 IgG H&L (abcam, ab150077) as a secondary antibody at room temperature for 1 hour. the cells and sections
376 were enclosed using ProLong Glass Antifade Mountant (Thermo Fisher Scientific) after staining the nuclei
377 with 4' ,6-diamidino-2-phenylindole (DAPI) at room temperature for 5 min. The fluorescent images were
378 obtained under a fluorescence microscope (Keyence).

379 *Cell proliferation assay*

380 C2C12 myoblasts were seeded in 96-well plates at 5,000 cells/well with 1mM 4-PBA or DMSO. After
381 incubated for 24, 48, and 72 hours, cell proliferation was measured using Cell Titer 96 AQueous Assay Kit
382 (Promega) according to the manufacturer's instructions.

383 *Quantitative real time Polymerase Chain Reaction (qPCR)*

384 Total RNA was prepared using the ISOSPIN Cell & Tissue RNA (Nippon Gene) and was transcribed into
385 cDNA using the ReverTra Ace qPCR RT Master Mix with gRNA remover (Toyobo). The qPCR was
386 performed using PowerTrack SYBR Green Master Mix for qPCR (Thermo Fisher Scientific, A46109) with
387 specific forward and reverse primers in a QuantStudio3 (Thermo Fisher Scientific). The relative gene
388 expression was calculated with the ΔΔCt method[56] (Livak and Schmittgen, 2001), using GAPDH or Actin
389 for normalization. See Table S2 for qPCR primer details.

390 *Chromatin immunoprecipitation (ChIP) - qPCR*

391 ChIP DNA was obtained using The SimpleChIP Enzymatic Chromatin IP Kit (Cell Signaling Technology
392 9003) according to the manufacturer's instructions. Briefly, 4×10^6 C2C12 cells were treated with 4% PFA
393 for 15 min for cross-link, and then with ultrasonic for shearing DNA into 500-bp of fragments. The
394 immunoprecipitation was implemented with 30 μL magnetic beads for 2 hours, following overnight
395 incubation of anti-p65 or control IgG antibodies. The collected precipitated chromatin was subjected to
396 qPCR. See Table S3 for ChIP-qPCR for primer details.

397 *Quantification and statistical analysis*

398 Statistical analysis were performed using R software (v4.5.1). We used Student's t-test to compare
399 differences between two samples. We also used one-way ANOVA and Tukey-Kramer test for differences
400 between the variances of the three groups. Values are presented as means ± S.E.M.

401 Visualized and analyses were performed using the following packages: clusterProfiler (version 4.16.0),
402 KEGGREST (version 1.48.1), and GO.db (version 3.21.0), ggplot2 (version 4.0.0), ggpubr (version 0.6.1),
403 pheatmap (version 1.0.13), VennDiagram (version 1.7.3), org.Mm.eg.db (version 3.21.0) from
404 Bioconductor (Huber W Nat Methods).

405 Gene Ontology (GO) enrichment analysis was performed using GO annotations[57]. Biological process terms
406 were tested for enrichment using a hypergeometric test, and p-values were adjusted for multiple testing
407 using the Benjamini-Hochberg method. GO terms with an adjusted p-value < 0.05 were considered

408 significant. KEGG pathway enrichment analysis was evaluated using a hypergeometric test with all
409 expressed genes as the background gene set[58] . P-values were adjusted using the Benjamini-Hochberg
410 method, and adjusted p-values < 0.05 were considered significant.

411

412 **Acknowledgments:** We thank T. Ogata for helping in RNA-seq data analysis and A. Kobayashi for
413 supporting general lab work. We thank Science Research Center, Insutitute of Life Science and Medicine
414 for animal research, and the Yamaguchi University Center for Gene Research for using Flow cytometry,
415 Imaging system, Microplate reader, and Real-time PCR system. This work was supported by Astellas
416 Foundation for Research on Metabolic Disorders (K.T.), Uehara Memorial Foundation (K.T.), New
417 Frontier Research Grant by Yamaguchi University (K.T., N.T.), Finding-Out & Crystallization of
418 Subliminals (FOCS) project by Yamaguchi University of Medicine (K.T., N.T.). This work was supported
419 in part by a Grant-in-Aid for Research Activity Start-up (21K21219), Early-Career Scientists (22K17826)
420 from Japan Society of the Promotion of Science (JSPS) (N.T.), ACT-X (JPMJAX222B) from Japan
421 Science and Technology Agency (JST) (N.T.), the Ube City Next-Generation Researchers Project (N.T.).
422 This work was the result of using research equipment shared in MEXT Project for promoting public
423 utilization of advanced research infrastructure (Program for supporting construction of core facilities),
424 Grant Number JPMXS0440400023.

425 **Author contributions:** K.T. conceived and designed the study. K.T. and N.T. performed experiments and
426 did the data analysis and interpretation. K.T. wrote the manuscript and prepared the figures. K.T. and N.T.
427 reviewed and edited the paper.

428 **Competing interests**: The author N.T. is a founder and director of ADDVEMO Inc.. ADDVEMO Inc. was
429 not involved in the study design, data collection, analysis, interpretation of data, the writing of the report,
430 or the decision to submit the article for publication. The author N.T. receives research funding from Otsuka
431 Electronics Co. for this study. The author K.T. declares no competing interests.

Data availability: RNA-seq data were deposited to GEO (GEO: GSE315556). All data in this published article (and its Supplementary Information files) are available.

Reference:

1. Yablonka-Reuveni, Z., Balestreri, T.M., and Bowen-Pope~, D.E. Regulation of Proliferation and Differentiation of Myoblasts Derived from Adult Mouse Skeletal Muscle by Specific Isoforms of PDGF.
2. Price, F.D., Matyas, M.N., Gehrke, A.R., Chen, W., Wolin, E.A., Holton, K.M., Gibbs, R.M., Lee, A., Singu, P.S., Sakakeeny, J.S., et al. (2025). Organoid culture promotes dedifferentiation of mouse myoblasts into stem cells capable of complete muscle regeneration. Nat. Biotechnol. *43*, 889–903. https://doi.org/10.1038/s41587-024-02344-7.
3. Motohashi, N., and Asakura, A. (2014). Muscle satellite cell heterogeneity and self-renewal. Preprint at Frontiers Media S.A., https://doi.org/10.3389/fcell.2014.00001 https://doi.org/10.3389/fcell.2014.00001.
4. Mourikis, P., and Relaix, F. (2016). Activated Muscle Satellite Cells Chase Ghosts. Preprint at Cell Press, https://doi.org/10.1016/j.stem.2016.01.008 https://doi.org/10.1016/j.stem.2016.01.008.
5. Dumont, N.A., Wang, Y.X., and Rudnicki, M.A. (2015). Intrinsic and extrinsic mechanisms regulating satellite cell function. Preprint at Company of Biologists Ltd, https://doi.org/10.1242/dev.114223 https://doi.org/10.1242/dev.114223.
6. Bentzinger (2010). Extrinsic regulation of satellite cell specification.
7. Berardi, E. (2017). Muscular dystrophies and cancer cachexia: Similarities in chronic skeletal muscle degeneration. Preprint at MDPI Multidisciplinary Digital Publishing Institute, https://doi.org/10.3390/jfmk2040039 https://doi.org/10.3390/jfmk2040039.

455 8. Chang, N.C., Chevalier, F.P., and Rudnicki, M.A. (2016). Satellite Cells in Muscular Dystrophy -
456 Lost in Polarity. Preprint at Elsevier Ltd, https://doi.org/10.1016/j.molmed.2016.04.002
457 https://doi.org/10.1016/j.molmed.2016.04.002.
458 9. Liang, D., Chen, C., Huang, S., Liu, S., Fu, L., and Niu, Y. (2022). Alterations of Lysine
459 Acetylation Profile in Murine Skeletal Muscles Upon Exercise. Front. Aging Neurosci. *14*.
460 https://doi.org/10.3389/fnagi.2022.859313.
461 10. Sincennes, M.-C., Brun, C.E., and Rudnicki, M.A. (2016). Concise Review: Epigenetic Regulation
462 of Myogenesis in Health and Disease. Stem Cells Transl. Med. *5*, 282–290.
463 https://doi.org/10.5966/sctm.2015-0266.
464 11. Timothy A McKinsey, C.L.Z. and E.N.O. (2001). Control of muscle development by dueling
465 HATs and HDACs. Curr. Opin. Genet. Dev., 497–504.
466 12. Li, Y., Khilji, S., Mach, Y.Z., Chen, J., and Li, Q. (2022). Chromatin state distribution of residue-
467 specific histone acetylation in early myoblast differentiation. J. Big Data *9*.
468 https://doi.org/10.1186/s40537-022-00667-3.
469 13. Massenet, J., Gardner, E., Chazaud, B., and Dilworth, F.J. (2021). Epigenetic regulation of
470 satellite cell fate during skeletal muscle regeneration. Preprint at BioMed Central Ltd,
471 https://doi.org/10.1186/s13395-020-00259-w https://doi.org/10.1186/s13395-020-00259-w.
472 14. Khilji, S., Hamed, M., Chen, J., and Li, Q. (2018). Loci-specific histone acetylation profiles
473 associated with transcriptional coactivator p300 during early myoblast differentiation. Epigenetics
474 *13*, 642–654. https://doi.org/10.1080/15592294.2018.1489659.
475 15. Hamed, M., Khilji, S., Chen, J., and Li, Q. (2013). Stepwise acetyltransferase association and
476 histone acetylation at the Myod1 locus during myogenic differentiation. Sci. Rep. *3*.
477 https://doi.org/10.1038/srep02390.
478 16. Pier Lorenzo Puri, S.I.P.S.T.-T.C.R.L.S.G.E.O.M.A.G.L.K.J.Y.J.W. and V.S. (2001). Class I
479 Histone Deacetylases Sequentially Interact with MyoD and pRb during Skeletal Myogenesis. Mol.
480 Cell *8*, 885–897.

481 17. Núñez-Álvarez, Y., Hurtado, E., Muñoz, M., García-Tuñon, I., Rech, G.E., Pluvinet, R., Sumoy,
482 L., Pendás, A.M., Peinado, M.A., and Suelves, M. (2021). Loss of HDAC11 accelerates skeletal
483 muscle regeneration in mice. FEBS Journal *288*, 1201–1223. https://doi.org/10.1111/febs.15468.
484 18. Mozzetta, C., Sartorelli, V., Steinkuhler, C., and Puri, P.L. (2024). HDAC inhibitors as
485 pharmacological treatment for Duchenne muscular dystrophy: a discovery journey from bench to
486 patients. Preprint at Elsevier Ltd, https://doi.org/10.1016/j.molmed.2024.01.007
487 https://doi.org/10.1016/j.molmed.2024.01.007.
488 19. Kolb, P.S., Ayaub, E.A., Zhou, W., Yum, V., Dickhout, J.G., and Ask, K. (2015). The therapeutic
489 effects of 4-phenylbutyric acid in maintaining proteostasis. Preprint at Elsevier Ltd,
490 https://doi.org/10.1016/j.biocel.2015.01.015 https://doi.org/10.1016/j.biocel.2015.01.015.
491 20. Lichter-Konecki, U., Diaz, G.A., Merritt, J.L., Feigenbaum, A., Jomphe, C., Marier, J.F.,
492 Beliveau, M., Mauney, J., Dickinson, K., Martinez, A., et al. (2011). Ammonia control in children
493 with urea cycle disorders (UCDs); Phase 2 comparison of sodium phenylbutyrate and glycerol
494 phenylbutyrate. Mol. Genet. Metab. *103*, 323–329. https://doi.org/10.1016/j.ymgme.2011.04.013.
495 21. Luo, T., Chen, B., and Wang, X. (2015). 4-PBA prevents pressure overload-induced myocardial
496 hypertrophy and interstitial fibrosis by attenuating endoplasmic reticulum stress. Chem. Biol.
497 Interact. *242*, 99–106. https://doi.org/10.1016/j.cbi.2015.09.025.
498 22. Mimori, S., Ohtaka, H., Koshikawa, Y., Kawada, K., Kaneko, M., Okuma, Y., Nomura, Y.,
499 Murakami, Y., and Hamana, H. (2013). 4-Phenylbutyric acid protects against neuronal cell death
500 by primarily acting as a chemical chaperone rather than histone deacetylase inhibitor. Bioorg.
501 Med. Chem. Lett. *23*, 6015–6018. https://doi.org/10.1016/j.bmcl.2013.08.001.
502 23. De Almeida, S.F., Picarote, G., Fleming, J. V., Carmo-Fonseca, M., Azevedo, J.E., and De Sousa,
503 M. (2007). Chemical chaperones reduce endoplasmic reticulum stress and prevent mutant HFE
504 aggregate formation. Journal of Biological Chemistry *282*, 27905–27912.
505 https://doi.org/10.1074/jbc.M702672200.

506 24. Rubenstein, R.C., Egan, M.E., and Zeitlin, P.L. (1997). In vitro pharmacologic restoration of
507 CFTR-mediated chloride transport with sodium 4-phenylbutyrate in cystic fibrosis epithelial cells
508 containing ΔF08-CFTR. Journal of Clinical Investigation *100*, 2457–2465.
509 https://doi.org/10.1172/JCI119788.
510 25. Rubenstein, R.C., and Zeitlin, P.L. (1998). A Pilot Clinical Trial of Oral Sodium 4-Phenylbutyrate
511 (Buphenyl) in F508-Homozygous Cystic Fibrosis Patients Partial Restoration of Nasal Epithelial
512 CFTR Function.
513 26. Omar, R., Lee, M.A.W., Gonzalez-Trueba, L., Thomson, C.R., Hansen, U., Lianos, S., Hazarika,
514 S., El Abdallah, O. El, Ammar, M.A., Cassels, J., et al. (2025). The chemical chaperone 4-
515 phenylbutyric acid rescues molecular cell defects of COL3A1 mutations that cause vascular Ehlers
516 Danlos Syndrome. Cell Death Discov. *11*. https://doi.org/10.1038/s41420-025-02476-y.
517 27. Tominaga, K., Tominaga, N., Williams, E.O., Rufibach, L., Schöwel, V., Spuler, S., Viswanathan,
518 M., and Guarente, L.P. (2022). 4-Phenylbutyrate restores localization and membrane repair to
519 human dysferlin mutations. iScience *25*. https://doi.org/10.1016/j.isci.2021.103667.
520 28. Li, Y., Weng, X., Wang, P., He, Z., Cheng, S., Wang, D., Li, X., Cheng, G., and Li, T. (2021). 4-
521 phenylbutyrate exerts stage-specific effects on cardiac differentiation via HDAC inhibition. PLoS
522 One *16*. https://doi.org/10.1371/journal.pone.0250267.
523 29. Shi, X., Gong, L., Liu, Y., Hou, K., Fan, Y., Li, C., Wen, T., Qu, X., and Che, X. (2020). 4-
524 phenylbutyric acid promotes migration of gastric cancer cells by histone deacetylase inhibition-
525 mediated IL-8 upregulation. Epigenetics *15*, 632–645.
526 https://doi.org/10.1080/15592294.2019.1700032.
527 30. Kusaczuk, M., Krętowski, R., Bartoszewicz, M., and Cechowska-Pasko, M. (2016).
528 Phenylbutyrate—a pan-HDAC inhibitor—suppresses proliferation of glioblastoma LN-229 cell
529 line. Tumor Biology *37*, 931–942. https://doi.org/10.1007/s13277-015-3781-8.

530 31. Shanmugam, G., Rakshit, S., and Sarkar, K. (2022). HDAC inhibitors: Targets for tumor therapy,
531 immune modulation and lung diseases. Preprint at Neoplasia Press, Inc.,
532 https://doi.org/10.1016/j.tranon.2021.101312 https://doi.org/10.1016/j.tranon.2021.101312.
533 32. Zhou, Y., Jin, X., Yu, H., Qin, G., Pan, P., Zhao, J., Chen, T., Liang, X., Sun, Y., Wang, B., et al.
534 (2022). HDAC5 modulates PD-L1 expression and cancer immunity via p65 deacetylation in
535 pancreatic cancer. Theranostics *12*, 2080–2094. https://doi.org/10.7150/thno.69444.
536 33. Hu, H., Li, L., Wang, C., He, H., Mao, K., Ma, X., Shi, R., Oh, Y., Zhang, F., Lu, Y., et al. (2014).
537 4-phenylbutyric acid increases GLUT4 gene expression through suppression of HDAC5 but not
538 endoplasmic reticulum stress. Cellular Physiology and Biochemistry *33*, 1899–1910.
539 https://doi.org/10.1159/000362967.
540 34. Dunham, I., Kundaje, A., Aldred, S.F., Collins, P.J., Davis, C.A., Doyle, F., Epstein, C.B., Frietze,
541 S., Harrow, J., Kaul, R., et al. (2012). An integrated encyclopedia of DNA elements in the human
542 genome. Nature *489*, 57–74. https://doi.org/10.1038/nature11247.
543 35. Nadine Bakkar, D.C.G. (2010). NF-B Signaling: A Tale of Two Pathways in Skeletal Myogenesis.
544 Physiol. Rev. *90*, 495–511. https://doi.org/10.1152/physrev.00040.2009.-NF-B.
545 36. Acharyya, S., Villalta, S.A., Bakkar, N., Bupha-Intr, T., Janssen, P.M.L., Carathers, M., Li, Z.W.,
546 Beg, A.A., Ghosh, S., Sahenk, Z., et al. (2007). Interplay of IKK/NF-κB signaling in macrophages
547 and myofibers promotes muscle degeneration in Duchenne muscular dystrophy. Journal of
548 Clinical Investigation *117*, 889–901. https://doi.org/10.1172/JCI30556.
549 37. Bakkar, N., Wang, J., Ladner, K.J., Wang, H., Dahlman, J.M., Carathers, M., Acharyya, S.,
550 Rudnicki, M.A., Hollenbach, A.D., and Guttridge, D.C. (2008). IKK/NF-κB regulates skeletal
551 myogenesis via a signaling switch to inhibit differentiation and promote mitochondrial biogenesis.
552 Journal of Cell Biology *180*, 787–802. https://doi.org/10.1083/jcb.200707179.
553 38. Guttridge, D.C., Albanese, C., Reuther, J.Y., Pestell, R.G., and Baldwin, A.S. (1999). NF-B
554 Controls Cell Growth and Differentiation through Transcriptional Regulation of Cyclin D1.

555 39. Lee, D., and Goldberg, A.L. (2015). Muscle wasting in fasting requires activation of NF-κB and
556 inhibition of AKT/Mechanistic target of rapamycin (mTOR) by the protein acetylase, GCN5.
557 Journal of Biological Chemistry *290*, 30269–30279. https://doi.org/10.1074/jbc.M115.685164.
558 40. Pryce, B.R., Oles, A., Talbert, E.E., Romeo, M.J., Vaena, S., Sharma, S., Spadafora, V., Tolliver,
559 L., Mahvi, D.A., Morgan, K.A., et al. (2024). Muscle inflammation is regulated by NF-κB from
560 multiple cells to control distinct states of wasting in cancer cachexia. Cell Rep. *43*.
561 https://doi.org/10.1016/j.celrep.2024.114925.
562 41. MARIA KARALAKI, S.F.A.P. and M.K. (2009). Muscle Regeneration: Cellular and Molecular
563 Events. In Vivo (Brooklyn). *23*, 779–796.
564 42. Zhang, W., Liu, Y., and Zhang, H. (2021). Extracellular matrix: an important regulator of cell
565 functions and skeletal muscle development. Preprint at BioMed Central Ltd,
566 https://doi.org/10.1186/s13578-021-00579-4 https://doi.org/10.1186/s13578-021-00579-4.
567 43. Sáenz, A., Azpitarte, M., Armañanzas, R., Leturcq, F., Alzualde, A., Inza, I., García-Bragado, F.,
568 De la Herran, G., Corcuera, J., Cabello, A., et al. (2008). Gene expression profiling in limb-girdle
569 muscular dystrophy 2A. PLoS One *3*. https://doi.org/10.1371/journal.pone.0003750.
570 44. Rizzo, B., Dragoni, F., Dainesi, M.I., Di Gerlando, R., Minucchi, E., Berardinelli, A.L., and
571 Gagliardi, S. (2025). Comparative Transcriptomic Profiling in Patients Affected by Duchenne and
572 Becker Muscular Dystrophies: A Focus on ECM Genes Dysregulation. Int. J. Mol. Sci. *26*.
573 https://doi.org/10.3390/ijms26146594.
574 45. Smith, L.R., Hammers, D.W., Sweeney, H.L., and Barton, E.R. (2016). Increased collagen cross-
575 linking is a signature of dystrophin-deficient muscle. Muscle Nerve *54*, 71–78.
576 https://doi.org/10.1002/mus.24998.
577 46. Ieronimakis, N., Hays, A., Prasad, A., Janebodin, K., Duffield, J.S., and Reyes, M. (2016).
578 PDGFRα signalling promotes fibrogenic responses in collagen-producing cells in Duchenne
579 muscular dystrophy. Journal of Pathology *240*, 410–424. https://doi.org/10.1002/path.4801.

47. Sanes, J.R. (2003). The basement membrane/basal lamina of skeletal muscle. Preprint, https://doi.org/10.1074/jbc.R200027200 https://doi.org/10.1074/jbc.R200027200.

48. Schüler, S.C., Liu, Y., Dumontier, S., Grandbois, M., Le Moal, E., Cornelison, D.D.W., and Bentzinger, C.F. (2022). Extracellular matrix: Brick and mortar in the skeletal muscle stem cell niche. Preprint at Frontiers Media S.A., https://doi.org/10.3389/fcell.2022.1056523 https://doi.org/10.3389/fcell.2022.1056523.

49. Hartwig, S., Raschke, S., Knebel, B., Scheler, M., Irmler, M., Passlack, W., Muller, S., Hanisch, F.G., Franz, T., Li, X., et al. (2014). Secretome profiling of primary human skeletal muscle cells. Biochim. Biophys. Acta Proteins Proteom. *1844*, 1011–1017. https://doi.org/10.1016/j.bbapap.2013.08.004.

50. Le Bihan, M.C., Bigot, A., Jensen, S.S., Dennis, J.L., Rogowska-Wrzesinska, A., Lainé, J., Gache, V., Furling, D., Jensen, O.N., Voit, T., et al. (2012). In-depth analysis of the secretome identifies three major independent secretory pathways in differentiating human myoblasts. J. Proteomics *77*, 344–356. https://doi.org/10.1016/j.jprot.2012.09.008.

51. Fox, M.A., Ho, M.S.P., Smyth, N., and Sanes, J.R. (2008). A synaptic nidogen: Developmental regulation and role of nidogen-2 at the neuromuscular junction. Neural Dev. *3*. https://doi.org/10.1186/1749-8104-3-24.

52. Deák, F., Mátés, L., Korpos, É., Zvara, Á., Szénási, T., Kiricsi, M., Mendler, L., Keller-Pintér, A., Ózsvári, B., Juhász, H., et al. (2014). Extracellular deposition of matrilin-2 controls the timing of the myogenic program during muscle regeneration. J. Cell Sci. *127*, 3240–3256. https://doi.org/10.1242/jcs.141556.

53. Zhao, X., Zhu, M., Wang, Z., Gao, M., Long, Y., Zhou, S., and Wang, W. (2025). The Alleviative Effect of Sodium Butyrate on Dexamethasone-Induced Skeletal Muscle Atrophy. Cell Biol. Int. *49*, 508–521. https://doi.org/10.1002/cbin.70003.

54. Chang, J.-G., Hsieh-Li, H.-M., Jong, Y.-J., Wang, N.M., Tsai, C.-H., and Li, H. (2001). Treatment of spinal muscular atrophy by sodium butyrate. Proc Natl Acad Sci U S A . *98*.

606 55. Bajanca, F., and Vandel, L. (2017). Epigenetic Regulators Modulate Muscle Damage in Duchenne
607 Muscular Dystrophy Model. PLoS Curr.
608 https://doi.org/10.1371/currents.md.f1e2379fa632f8135577333dd92ca83b.
609 56. Livak, K.J., and Schmittgen, T.D. (2001). Analysis of relative gene expression data using real-time
610 quantitative PCR and the 2-ΔΔCT method. Methods *25*, 402–408.
611 https://doi.org/10.1006/meth.2001.1262.
612 57. Ashburner, M., Ball, C.A., Blake, J.A., Botstein, D., Butler, H., Cherry, J.M., Davis, A.P.,
613 Dolinski, K., Dwight, S.S., Eppig, J.T., et al. (2000). Gene ontology: Tool for the unification of
614 biology. Preprint, https://doi.org/10.1038/75556 https://doi.org/10.1038/75556.
615 58. Kanehisa, M., and Goto, S. (2000). KEGG: Kyoto Encyclopedia of Genes and Genomes.
616

Figures

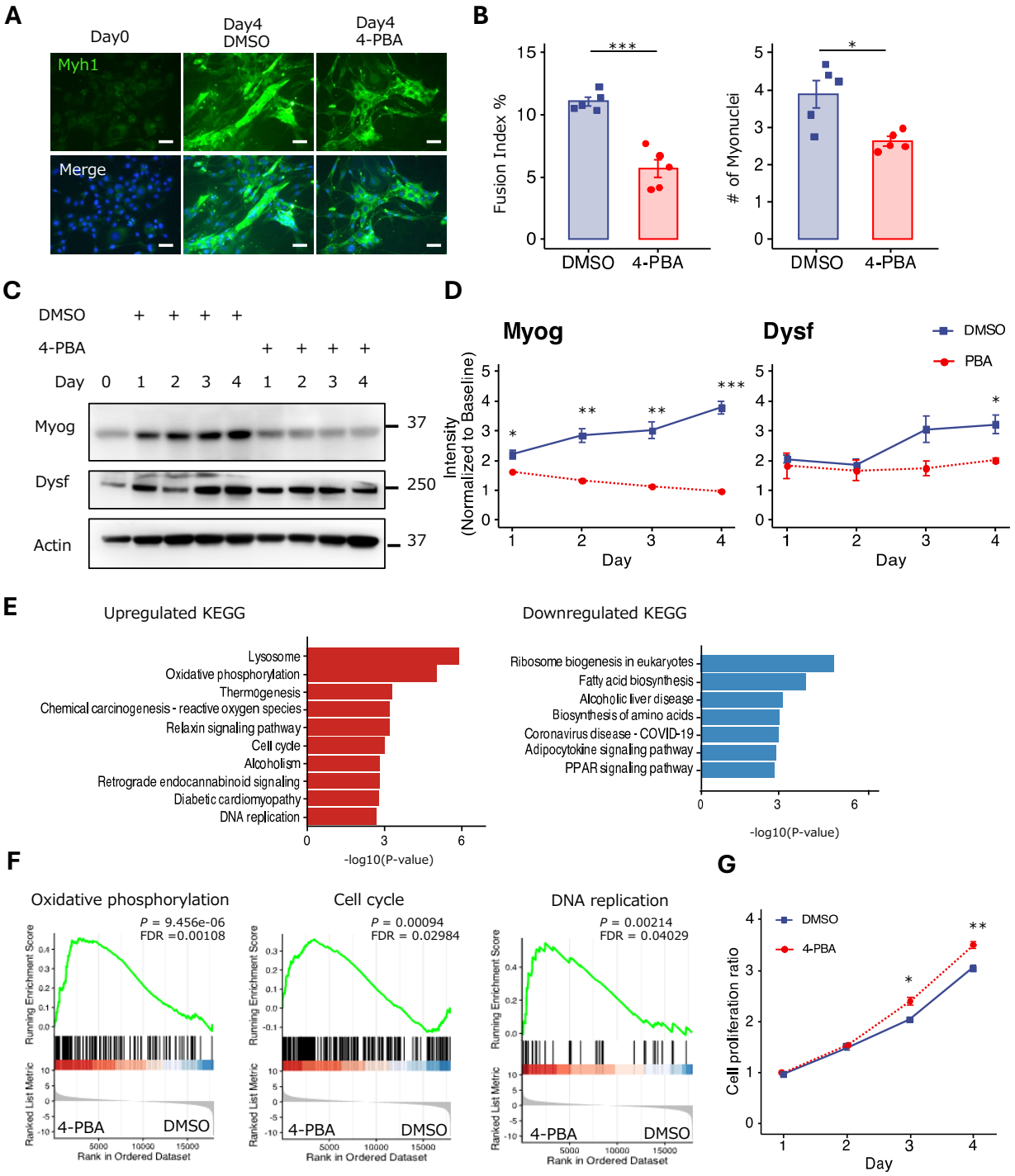

Figure 1. 4-PBA Promotes Myoblast Proliferation but Impairs Myogenic Differentiation.

(A) Representative immunofluorescence images of C2C12 myotubes stained for Myh1 (green) and nuclei (blue). Scale bar, 400 μm.

(B) (left) Quantification of Myh1^{+} myotube area per field 4 days after differentiation (n = 5). (right) the number of nuclei within multinucleated myotubes (n = 5).

(C) Representative immunoblots showing Myogenin (Myog) and Dysferlin (Dysf) expression in C2C12 cells treated with 1 mM 4-PBA or DMSO for the indicated time points.

(D) Quantification of Myog and Dysf protein levels shown in (C), normalized to β-actin (Actin). Data are representative of three independent experiments.

(E) KEGG pathway enrichment analysis of differentially expressed genes in C2C12 myotubes at day 4 after differentiation, comparing treatment with 1 mM 4-PBA and DMSO.

(F) Gene set enrichment analysis (GSEA) plots for the indicated KEGG pathways in 4-PBA– or DMSO-treated cells. FDR, false discovery rate.

(G) Proliferation of C2C12 myoblasts treated with 1 mM 4-PBA or DMSO.

Data in (B), (D) and (G) are presented as mean ± S.E.M. and analyzed using an unpaired two-tailed Student's t test. *$P < 0.05$, **$P < 0.01$, ***$P < 0.001$.

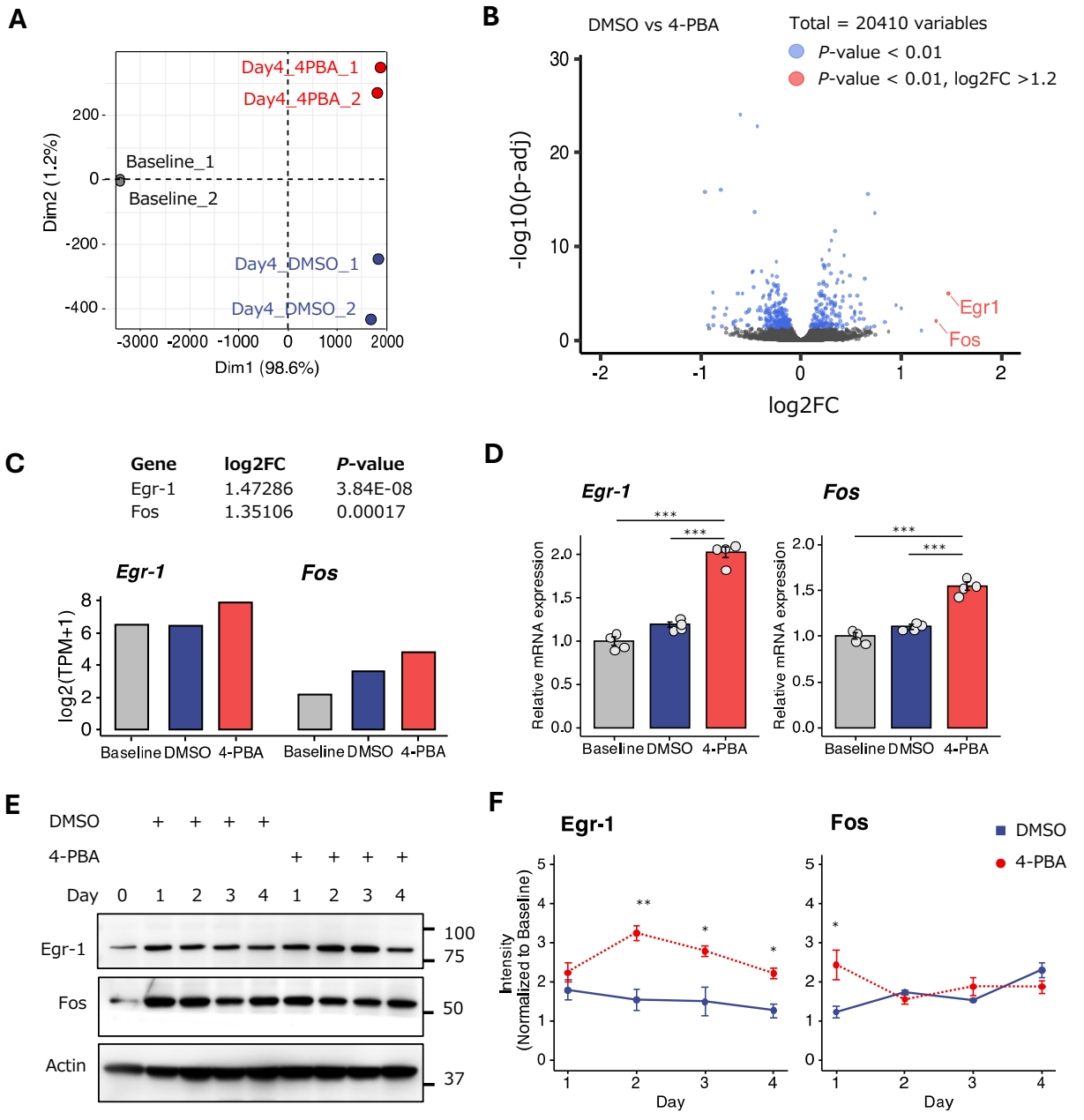

Figure 2. 4-PBA Induces Egr-1 Expression during Myoblast Differentiation.

(A) Principal component analysis (PCA) showing sample clustering based on differentially expressed genes in C2C12 cells treated with 1 mM 4-PBA or DMSO. Baseline indicates cells prior to differentiation induction.

(B) Volcano plot of differentially expressed genes identified by RNA-seq analysis comparing 4-PBA–treated and DMSO-treated C2C12 cells following myotube differentiation after 4 days. Significantly upregulated genes are shown in red. FC, fold change; P-adj, adjusted p value.

(C) RNA-seq–based expression levels of *Egr-1* and *Fos* mRNA in C2C12 cells treated with 1 mM 4-PBA or DMSO, shown as transcripts per million (TPM).

(D) Quantitative PCR (qPCR) validation of *Egr-1* and *Fos* mRNA expression in C2C12 cells treated with 1 mM 4-PBA or DMSO. Data represent four independent experiments.

(E) Representative immunoblots showing Egr-1 and Fos protein expression in C2C12 cells treated with 1 mM 4-PBA or DMSO for the indicated time points.

(F) Quantification of protein levels shown in (E), normalized to β-actin (Actin). Data represent three independent experiments.

Data in (D) and (F) are presented as mean ± S.E.M. and analyzed using one-way ANOVA with Tukey's post hoc test (D) and unpaired two-tailed Student's t test (F). $^{*}P < 0.05$, $^{**}P < 0.01$, $^{***}P < 0.001$.

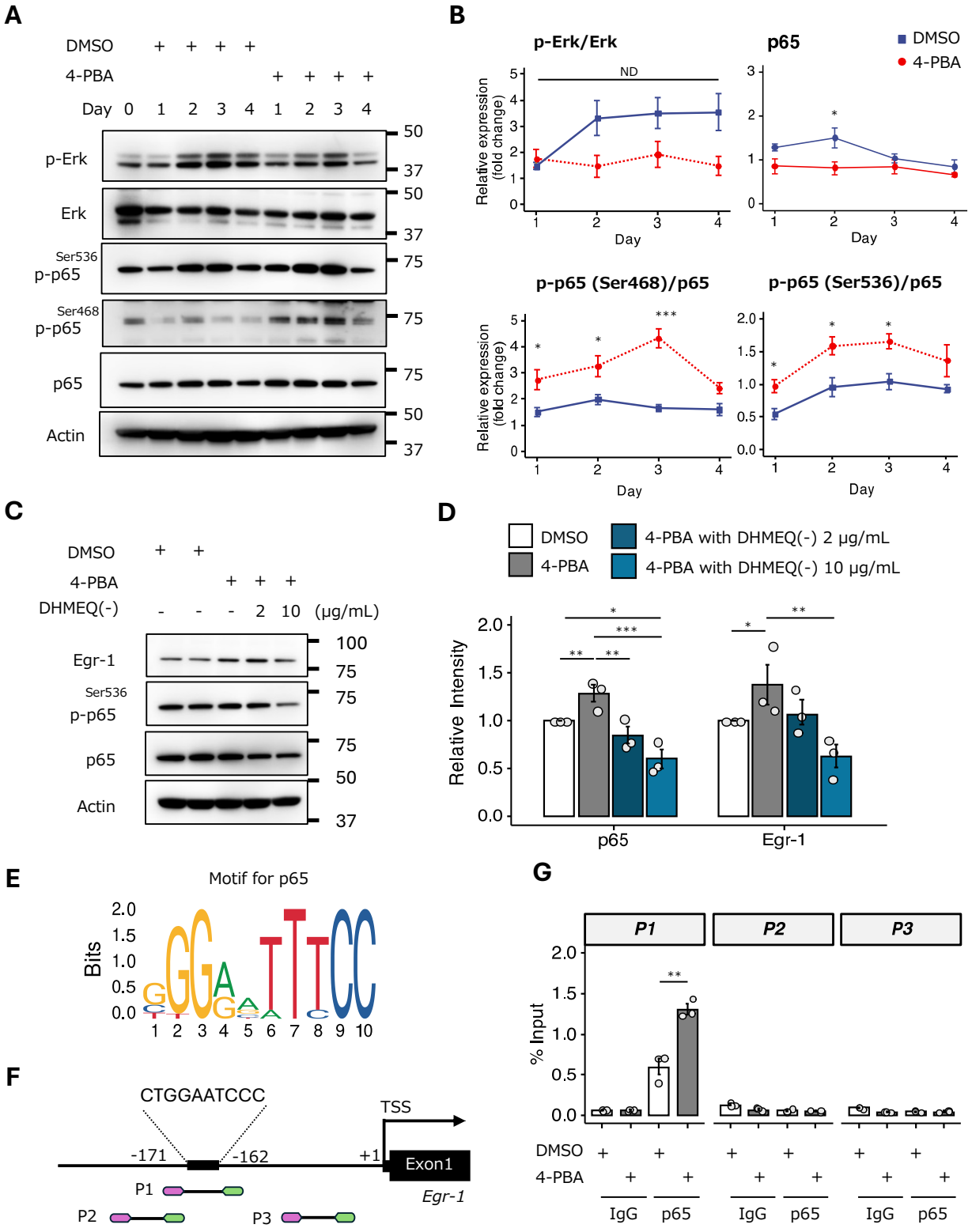

Figure 3. 4-PBA Regulates NF-κB–Dependent Egr-1 Expression in C2C12 Cells.

(A) Representative immunoblots showing total Erk1/2, phosphorylated Erk1/2 (Thr202/Tyr204), total p65, and phosphorylated p65 (Ser468 and Ser536) in C2C12 cells treated with 1 mM 4-PBA or DMSO for the indicated time points. β-actin (Actin) was used as a loading control.

(B) Quantification of phosphorylated Erk1/2 (Thr202/Tyr204) and phosphorylated p65 (Ser468 and Ser536) shown in (A). Band intensities were normalized to total Erk1/2 or p65, respectively. Data represent three independent experiments.

(C) Representative immunoblots showing Egr-1 and p65 protein levels in C2C12 cells treated with 1 mM 4-PBA in the presence or absence of the NF-κB inhibitor DHMEQ. Actin was used as a loading control.

(D) Quantification of Egr-1 and p65 protein levels shown in (C), normalized to Actin. Data represent three independent experiments.

(E) NF-κB p65 consensus binding motif predicted using the JASPAR database.

(F) Predicted p65 binding sites within the Egr-1 promoter region identified by JASPAR analysis.

(G) Chromatin immunoprecipitation (ChIP) analysis showing enrichment of the Egr-1 promoter regions (P1 and P2) in p65- or IgG-immunoprecipitated chromatin from 4-PBA–treated C2C12 cells.

Data in (B), (D) and (G) are presented as mean ± S.E.M. and analyzed using an unpaired two-tailed Student's t test (B) and one-way ANOVA with Tukey's post hoc test (D, G). $^{*}P < 0.05$, $^{**}P < 0.01$, $^{***}P < 0.001$; ns, not significant.

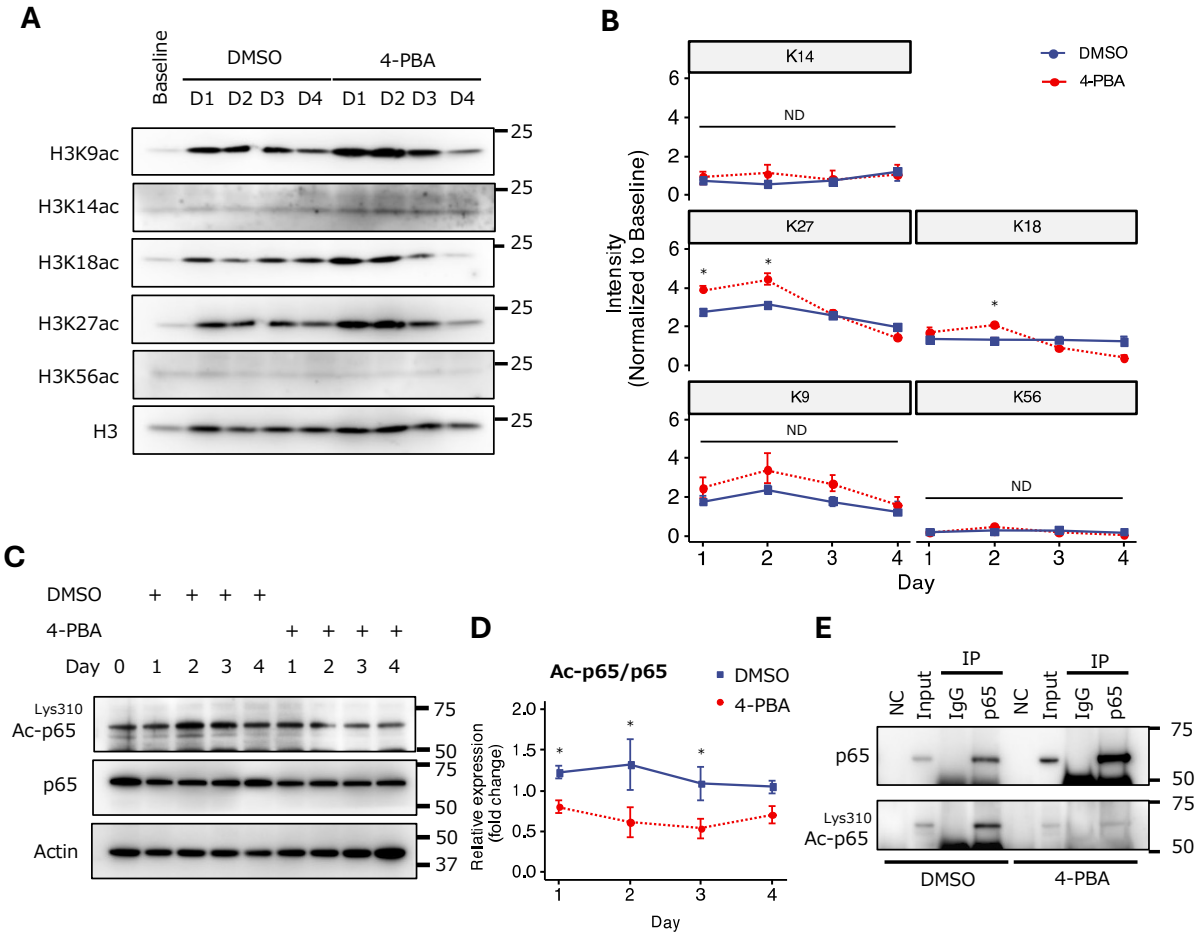

Figure 4. 4-PBA Induces Histone H3K27/18 Acetylation but Does Not Promote p65 Acetylation.

(A) Representative immunoblots showing acetylated histone H3 (H3K9/14/18/27/56ac) in C2C12 cells treated with 1 mM 4-PBA or DMSO for the indicated time points. Total histone H3 was used as a loading control.

(B) Quantification of histone H3K27/18 acetylation shown in (A), normalized to total histone H3. Data represent three independent experiments.

(C) Representative immunoblots showing total p65 and acetylated p65 (Lys310) in C2C12 cells treated with 1 mM 4-PBA or DMSO for the indicated time points. β-actin (Actin) was used as a loading control.

(D) Quantification of acetylated p65 (Lys310) levels shown in (C), normalized to Actin. Data represent three independent experiments.

(E) Immunoprecipitation of p65 from C2C12 cell lysates followed by immunoblot analysis with antibodies against total p65 or acetylated p65 (Lys310). Input lysates are shown as controls.

Data in (B) and (D) are presented as mean ± S.E.M. and analyzed using an unpaired two-tailed Student's t test (B, D). *$P < 0.05$; ns, not significant.

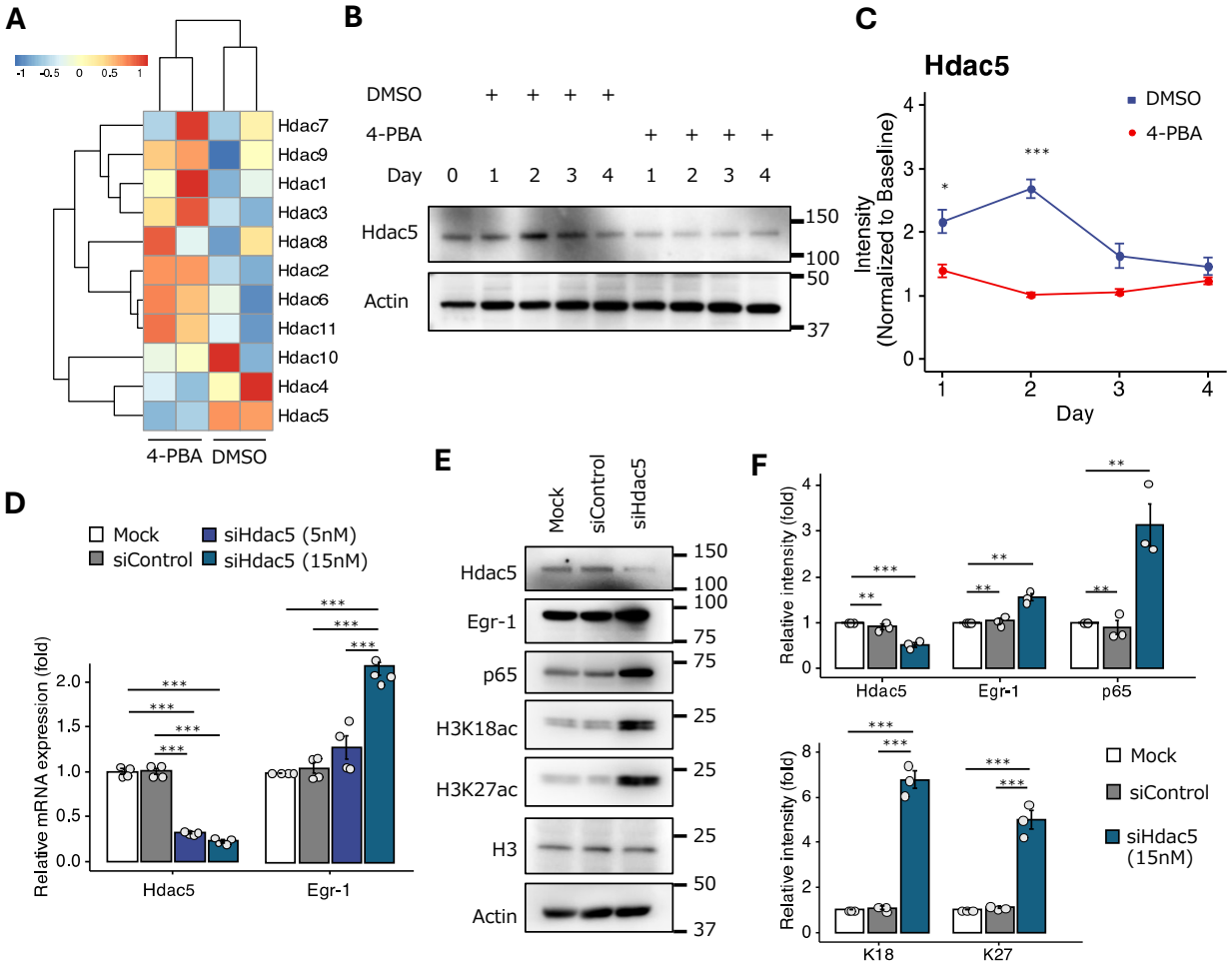

Figure 5. 4-PBA Regulates Egr-1 Expression through Suppression of HDAC5 in C2C12 Cells.

(A) Heatmap showing RNA-seq–based expression profiles of histone deacetylase (HDAC) genes in C2C12 cells treated with 1 mM 4-PBA or DMSO.

(B) Representative immunoblots showing HDAC5 protein levels in C2C12 cells treated with 1 mM 4-PBA or DMSO for the indicated time points. β-actin (Actin) was used as a loading control.

(C) Quantification of HDAC5 protein levels shown in (B), normalized to Actin. Data represent three independent experiments.

(D) Relative mRNA expression of *Hdac5* and *Egr-1* in C2C12 cells transfected with siHdac5 (5 or 15 nM), siControl, or mock control, as measured by qPCR. Expression levels were normalized to *β-actin* (*Actin*).

(E) Representative immunoblots showing HDAC5, Egr-1, p65, H3K18ac, and H3K27ac protein levels in C2C12 cells treated with 1 mM 4-PBA or DMSO for the indicated time points. Actin or histone H3 was used as the loading control, as indicated.

(F) Quantification of protein levels shown in (E). Band intensities were normalized to Actin for HDAC5, Egr-1, and p65, and to histone H3 for H3K18ac and H3K27ac. Data represent three independent experiments.

Data in (C), (D) and (F) are presented as mean ± S.E.M. and analyzed using an unpaired two-tailed Student's t test (C) and one-way ANOVA with Tukey's post hoc test (D, F). *$P < 0.05$, **$P < 0.01$, ***$P < 0.001$.

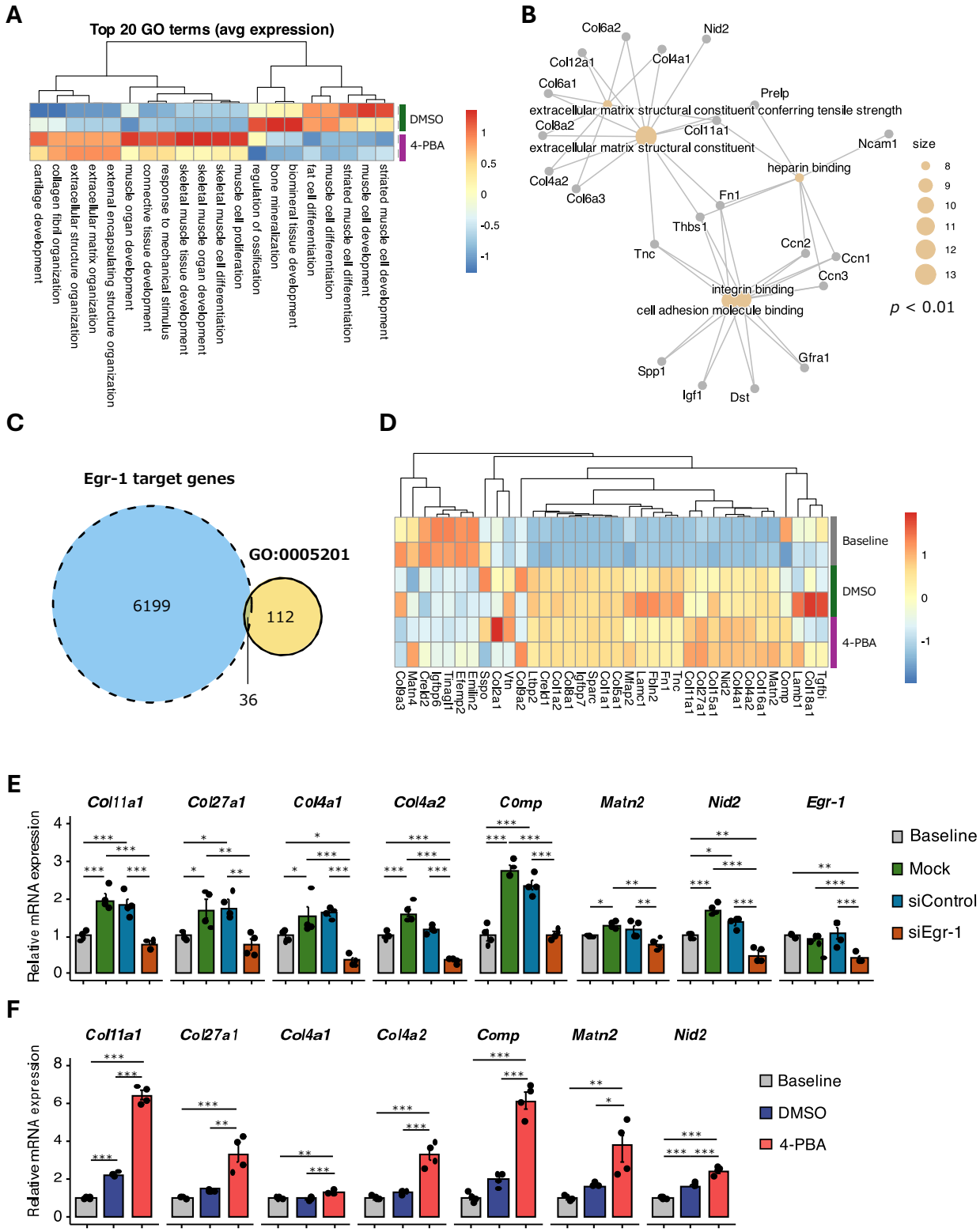

Figure 6. Egr-1 Mediates 4-PBA–Dependent Transcriptional Regulation of Extracellular Matrix Organization Genes.

(A) Heatmap of Gene Ontology (GO) hallmark gene sets with the top 20 lowest p values identified by parametric gene set enrichment analysis (GSEA) from RNA-seq data of C2C12 cells treated with 1 mM 4-PBA or DMSO.

(B) Network visualization illustrating the functional connectivity between differentially expressed genes (DEGs) and enriched biological processes, highlighting extracellular matrix (ECM) organization–related pathways regulated by 4-PBA. Node size corresponds to the number of genes within each enriched pathway.

(C) Venn diagram showing overlap between genes associated with the ECM structural constituent GO term (GO:0005201) and predicted Egr-1 target genes obtained from the ENCODE Transcription Factor Targets Dataset.

(D) Heatmap showing expression patterns of Egr-1 target genes within the ECM structural constituent gene set, demonstrating coordinated regulation downstream of 4-PBA treatment.

(E) Relative mRNA expression of selected ECM-related genes in C2C12 cells transfected with siEgr-1 (15 nM), siControl, or mock control, showing Egr-1–dependent transcriptional regulation. Expression levels were normalized to β-actin (Actin).

(F) Relative mRNA expression of selected ECM-related genes in C2C12 cells treated with 1 mM 4-PBA or DMSO under differentiation conditions. Baseline indicates expression levels prior to differentiation induction.

Data in (E) and (F) are presented as mean ± S.E.M. and analyzed using a one-way ANOVA with Tukey's post hoc test. $^{*}P < 0.05$, $^{**}P < 0.01$, $^{***}P < 0.001$.